

1 Time dependent intrinsic correlation analysis of  
2 temperature and dissolved oxygen time series using  
3 empirical mode decomposition

4 Yongxiang Huang<sup>a</sup>, François G. Schmitt<sup>b</sup>,

5 *<sup>a</sup>Shanghai Institute of Applied Mathematics and Mechanics, Shanghai Key Laboratory  
6 of Mechanics in Energy Engineering, Shanghai University, Shanghai 200072, People's  
7 Republic of China*

8 *<sup>b</sup>CNRS and University of Lille 1, Laboratory of Oceanology and Geosciences, UMR  
9 8187 LOG, 62930 Wimereux, France*

---

10 **Abstract**

In the marine environment, many fields have fluctuations over a large range of different spatial and temporal scales. These quantities can be nonlinear and non-stationary, and often interact with each other. A good method to study the multiple scale dynamics of such time series, and their correlations, is needed. In this paper an application of an empirical mode decomposition based time dependent intrinsic correlation, of two coastal oceanic time series, temperature and dissolved oxygen (saturation percentage) is presented. The two time series are recorded every 20 minutes for 7 years, from 2004 to 2011. The application of the Empirical Mode Decomposition on such time series is illustrated, and the power spectra of the time series are estimated using the Hilbert transform (Hilbert spectral analysis). Power-law regimes are found with slopes of 1.33 for dissolved oxygen and 1.68 for temperature at high frequencies (between 1.2 and 12 hours) with both close to 1.9 for lower frequencies (time scales from 2 to 100 days). Moreover, the time evolution and scale dependence of cross correlations be-

tween both series are considered. The trends are perfectly anti-correlated. The modes of mean year 3 and 1 year have also negative correlation, whereas higher frequency modes have a much smaller correlation. The estimation of time-dependent intrinsic correlations helps to show patterns of correlations at different scales, for different modes.

<sup>11</sup> *Keywords:* Coastal oceanic time series, Oceanic temperature, Oceanic  
<sup>12</sup> dissolved oxygen, Empirical Mode Decomposition, Hilbert Spectral  
<sup>13</sup> Analysis, cross correlation.

---

---

*Email addresses:* [yongxianghuang@gmail.com](mailto:yongxianghuang@gmail.com) (Yongxiang Huang),  
[francois.schmitt@univ-lille1.fr](mailto:francois.schmitt@univ-lille1.fr) (François G. Schmitt)

## 14 **1. Introduction**

15       Generally in geosciences, but especially in the marine environment, many  
16 fields have fluctuations over a large range of spatial and temporal scales. To  
17 study their dynamics and estimate their variations at all scales, high fre-  
18 quency measurements are needed (Dickey, 1991; Chavez, 1997; Chang and Dickey,  
19 2001). Here a time series obtained from automatic measurements in a  
20 moored buoy station in coastal waters of Boulogne-sur-mer (eastern En-  
21 glish Channel, France) is considered, recorded every 20 minutes from 2004  
22 to 2011 (Zongo and Schmitt, 2011; Zongo et al., 2011). This fixed buoy sta-  
23 tion can record various biogeochemical parameters simultaneously. Here,  
24 mainly to illustrate the application of a new method for multi-scale data  
25 analysis there is a focus on two parameters: temperature, due to its obvious  
26 importance, influenced by the dynamics, by meteorology, and as a link with  
27 ecosystem forcing, and dissolved oxygen time series, due to its important  
28 role in biological processes, and also for the probable growing importance  
29 of this parameter to assess the quality of coastal waters, in the framework  
30 of European directives (Best et al., 2007).

31       These physical and biogeochemical time series are nonlinear, and non-  
32 stationary, and may possess interactions at different scales. In order to  
33 consider their multi-scale dynamic properties and explore their correlations  
34 at different scales, the Empirical Mode Decomposition (EMD) framework  
35 is applied here (Huang et al., 1998).

36       EMD and the associated Hilbert spectral analysis (resp. Hilbert-Huang  
37 Transform, HHT) have already been applied in marine sciences, (Hwang et al.,  
38 2003; Dätig and Schlurmann, 2004; Veltcheva and Soares, 2004; Schmitt et al.,  
39 2009). For example, Hwang et al. (2003) applied the HHT method to ocean

40 wave data. They found that the HHT method detects more energy in lower  
41 frequencies, leading to a lower average frequency in HHT spectra than us-  
42 ing the Fourier framework. Dätig and Schlurmann (2004) showed that the  
43 HHT method can be used to study nonlinear waves using instantaneous fre-  
44 quencies. Schmitt et al. (2009) applied the HHT method to characterize  
45 the scale invariance of velocity fluctuations in the surf zone. They observed  
46 that the scale invariance holds for almost two decades of time scales.

47 In the following, the methodology is presented and then its application  
48 is illustrated on the chosen time series. Section 2 presents the Hilbert-  
49 Huang Transform method and the fairly recent time dependent intrinsic  
50 correlation; section 3 presents the data base; section 4 presents the analysis  
51 of the intrinsic correlation and section 5 draws the main conclusion of this  
52 paper.

## 53 **2. Hilbert-Huang Transform and Time Dependent Intrinsic Cor-** 54 **relation**

55 In this section, the Hilbert-Huang Transform and the empirical mode de-  
56 composition based time dependent intrinsic correlation are presented. These  
57 time series analysis techniques have been applied, since their introduction  
58 in 1998 (Huang et al., 1998), in several thousand different studies in natural  
59 and applied sciences. Here the main idea is recalled but the method is not  
60 presented in too much detail.

61 The HHT consists of two steps. The first step is the so-called ‘empirical  
62 mode decomposition’, which separates a multi-scale time series into a sum  
63 of intrinsic mode functions without *a priori* basis assumption (Huang et al.,  
64 1998; Flandrin and Gonçalves, 2004). In the second step, the Hilbert spec-

65 tral analysis is applied to each mode function to extract the time-frequency  
66 information. The so-called Hilbert spectrum and the corresponding Hilbert  
67 marginal spectrum are then introduced to characterize the time-frequency  
68 distribution of a given time series (Huang et al., 1998; Huang, 2009; Huang et al.,  
69 2008; Chen et al., 2010).

### 70 *2.1. Empirical Mode Decomposition*

71 Empirical Mode Decomposition is a fully adaptive technique to study  
72 the nonlinear and non-stationary properties of time series (Huang et al.,  
73 1998, 1999; Flandrin and Gonçalves, 2004; Huang et al., 2011). The main  
74 idea of EMD is to locally separate a given multi-scale signal into a sum  
75 of a local trend and a local detail, respectively, for a low frequency part  
76 and a high frequency part (Rilling et al., 2003). The latter is called the  
77 Intrinsic Mode Function (IMF), and the former is called the residual. The  
78 procedure is repeated to the residual, considered as a new times series,  
79 extracting a new IMF using a spline function, and obtaining a new residual  
80 until no more IMF can be extracted (Huang et al., 1998, 1999; Rilling et al.,  
81 2003; Flandrin et al., 2004). The EMD method then expresses a multi-  
82 scale time series as the sum of a finite number of IMFs and a final residual  
83 (Huang et al., 1998; Flandrin et al., 2004).

84 To be an IMF, an approximation to the so-called mono-component sig-  
85 nal, it must satisfy the following two conditions: (i) the difference between  
86 the number of local extrema and the number of zero-crossings must be zero  
87 or one; (ii) the running mean value of the envelope defined by the local max-  
88 ima and the envelope defined by the local minima is zero (Huang et al., 1998,  
89 1999; Rilling et al., 2003). The so-called Empirical Mode Decomposition al-

90 gorithm is then proposed to decompose a signal into IMFs (Huang et al.,  
91 1998, 1999; Rilling et al., 2003):

- 92 1 identify the local extrema of the signal  $x(t)$ ;
- 93 2 construct upper envelope  $e_{\max}(t)$  by using the local maxima through  
94 a cubic spline interpolation (other interpolations are also possible).  
95 Construct a lower envelope  $e_{\min}(t)$  by using the local minima;
- 96 3 define the mean value  $m_1(t) = (e_{\max}(t) + e_{\min}(t))/2$ ;
- 97 4 remove the mean value from the signal, providing the local detail  
98  $h_1(t) = x(t) - m_1(t)$ ;
- 99 5 check if the component  $h_1(t)$  satisfies the above conditions to be an  
100 IMF. If yes, take it as the first IMF  $C_1(t) = h_1(t)$ . This IMF mode is  
101 then removed from the original signal and the first residual,  $r_1(t) =$   
102  $x(t) - C_1(t)$  is taken as the new series in step 1. If  $h_1(t)$  is not an IMF,  
103 a procedure called the “sifting process” is applied as many times as  
104 necessary to obtain an IMF (not detailed here).

105 By construction, the number of extrema decreases when going from one  
106 residual to the next; the above algorithm ends when the residual has only  
107 one extrema, or is constant, and in this case no more IMF can be extracted;  
108 the complete decomposition is then achieved in a finite number of steps.  
109 The analyzed signal  $x(t)$  is finally written as the sum of mode time series  
110  $C_i(t)$  and the residual  $r_n(t)$ :

$$x(t) = \sum_{i=1}^N C_i(t) + r_n(t) \quad (1)$$

111 Based on a dyadic filter bank property of the EMD algorithm, the number  
 112 of IMF modes is estimated as

$$N \leq \log_2(L) \quad (2)$$

113 where  $L$  is the length of the data in points (Flandrin et al., 2004; Wu and Huang,  
 114 2004; Huang et al., 2008). Unlike Fourier based methodologies, e.g., Fourier  
 115 analysis, wavelet transform, etc., this method does not define the basis *a*  
 116 *priori* (Huang et al., 1998, 1999; Flandrin and Gonçalves, 2004). It thus  
 117 possesses full adaptability and is very suitable for non-stationary and non-  
 118 linear time series analysis (Huang et al., 1998, 1999).

## 119 2.2. Hilbert Spectral Analysis

120 To characterize the time-frequency distribution of the IMF mode, a com-  
 121plementary analysis technique namely Hilbert spectral analysis (HSA) is  
 122then applied to each IMF mode to extract the local frequency informa-  
 123tion (Long et al., 1995; Huang et al., 1998, 1999; Huang, 2009; Huang et al.,  
 1242011). In this complementary step, the Hilbert transform is used to con-  
 125struct the analytical signal, i.e.,

$$\tilde{C}(t) = C(t) + j\frac{1}{\pi}P \int_{-\infty}^{+\infty} \frac{C(t')}{t-t'} dt' \quad (3)$$

126 in which  $P$  is the Cauchy principle value (Cohen, 1995; Long et al., 1995;  
 127Huang et al., 1998; Flandrin, 1998). The above equation can be rewritten  
 128 as

$$\tilde{C}(t) = \mathcal{A}(t) \exp(j\theta(t)) \quad (4)$$

129 in which  $\mathcal{A}(t) = |\tilde{C}(t)|$  is the modulus and  $\theta(t) = \arctan(\text{IM}(\tilde{C}(t))/\text{RE}(\tilde{C}(t)))$   
 130 is the instantaneous phase function (Cohen, 1995; Long et al., 1995; Huang et al.,

131 1998; Flandrin, 1998; Huang, 2009; Huang et al., 2011). The instantaneous  
132 frequency is then defined as

$$\omega(t) = \frac{1}{2\pi} \frac{d\theta(t)}{dt} \quad (5)$$

133 Note that the instantaneous frequency  $\omega$  is very local since the Hilbert  
134 transform is a singularity transform and the differential operator is used  
135 to define the frequency  $\omega$  (Huang et al., 1998, 1999; Huang, 2009). It was  
136 found experimentally that the Hilbert-based methodology is free with the  
137 Heisenberg-Gabor uncertainty and can be used to describe nonlinear dis-  
138 tortions by using an intrawave-frequency-modulation mechanism, in which  
139 the frequency can be varied with time in one period (Huang et al., 1998;  
140 Huang, 2005; Huang et al., 2011). Therefore, the method is free with high-  
141 order harmonic components, which are required in Fourier-based methods  
142 to capture the non-stationary and nonlinear characteristics of the data  
143 (Huang et al., 1998, 1999; Huang, 2005; Huang et al., 2011).

144 Note that several methods exist, that could be applied to estimate the  
145 instantaneous frequency, e.g., direct quadrature, teager energy operator,  
146 etc.; see more detail in Huang et al. (2009a). In practice, the Hilbert method  
147 already provides a good estimation of  $\omega$  in a statistical sense (Huang et al.,  
148 2010, 2011).

149 A Hilbert spectrum  $H(\omega, t) = \mathcal{A}^2(\omega, t)$  can be designed to represent  
150 the energy of the original signal as a function of frequency  $\omega$  and time. It  
151 can be taken as the best local fit to  $x(t)$  using an amplitude and phase  
152 varying trigonometric function (Huang, 2005). This corresponds to a high  
153 resolution fit both in physical space and frequency space (Long et al., 1995;



154 Huang et al., 1998). Then, the Hilbert marginal  $h(\omega)$  can be defined as

$$h(\omega) = \frac{1}{T} \int_T H(\omega, t) dt \quad (6)$$

155 in which  $T$  is the time period to calculate the spectrum. This is compara-  
156 ble to the power spectrum in Fourier analysis, but it has a quite different  
157 definition and the resulting curve would be expected to be different from  
158 the Fourier  $E(f)$  curve if the times series is nonlinear and non-stationary  
159 (Huang et al., 1998). In fact, here the definition of instantaneous frequency  
160 is different from the one in the Fourier frame and the interpretation and  
161 detailed physical meaning of  $h(\omega)$  is still to be fully characterized.

162 Another way to estimate  $h(\omega)$  is based on the joint probability density  
163 function (pdf)  $p(\mathcal{A}, \omega)$  of amplitude  $\mathcal{A}$  and the instantaneous frequency  $\omega$   
164 from all IMF modes (Huang et al., 2008; Huang, 2009; Huang et al., 2010,  
165 2011). It is written as

$$h(\omega) = \int_{-\infty}^{+\infty} p(\mathcal{A}, \omega) \mathcal{A}^2 d\mathcal{A} \quad (7)$$

166 The combination of the EMD and HSA is then called Hilbert-Huang Trans-  
167 form (Huang, 2005). It has been applied successfully in various research  
168 fields to characterize the energy-time-frequency in different topics (Zhu et al.,  
169 1997; Echeverria et al., 2001; Coughlin and Tung, 2004; Loutridis, 2004;  
170 Jánosi and Müller, 2005; Molla et al., 2006a,b; Huang et al., 2008, 2009b;  
171 Schmitt et al., 2009; Chen et al., 2010), to cite a few.

### 172 *2.3. Time Dependent Intrinsic Correlation*

173 The classical global expression for the correlation, applied to non-stationary  
174 time series, may distort the true cross correlation information between time

175 series and provide unphysical interpretation (Hoover, 2003; Rodo and Rodriguez-Arias,  
176 2006; Chen et al., 2010). An alternative way, consistent with the possible  
177 non-stationarity of the time series, is to estimate the cross correlation co-  
178 efficient by using a sliding window or a scale dependent correlation tech-  
179 nique (Papadimitriou et al., 2006; Rodo and Rodriguez-Arias, 2006). But  
180 the main problem of these techniques is to determine how large the window  
181 should be (Chen et al., 2010). Time series from natural sciences possess fluc-  
182 tuations in a whole range of scales, and the data characterization must take  
183 into account this scale question (Cohen, 1995; Huang et al., 1998; Flandrin,  
184 1998). The estimation of the cross correlation between time series, in a  
185 multi-scale framework, may use a window based on the local characteristic  
186 scale given by the data itself.

187 Recently, Chen et al. (2010) proposed to use the EMD to estimate an  
188 adaptive window in order to calculate a so-called time-dependent intrinsic  
189 correlation (TDIC). The TDIC of each pair of IMFs is defined as follows:

$$R_{ij}(t_k^n | t_w^n) = \text{Corr}(C_{1,i}(t_w^n)C_{2,j}(t_w^n)) \text{ at any } t_k \quad (8)$$

190 where Corr is the cross correlation coefficient of two time series and  $t_w^n =$   
191  $[t_k - nt_d/2 : t_k + nt_d/2]$  is the sliding window. The minimum sliding window  
192 size for the local correlation estimation is chosen as  $t_d = \max(T_{1i}(t_k), T_{2j}(t_k))$ ,  
193 where  $T_{1i}$  and  $T_{2j}$  are the instantaneous periods  $T = \omega^{-1}$ , and  $n$  is any pos-  
194 itive real number (Chen et al., 2010). The efficiency of this approach to  
195 characterize the relation between two time series for several problems has  
196 been shown in Chen et al. (2010). Here we use this new method (with  
197  $n \geq 1$ ) to estimate cross correlations between coastal marine time series,  
198 where the latter can be considered as typical nonlinear and non-stationary

199 data.

### 200 **3. Presentation of the experimental database**

201 The time series analyzed here belong to the MAREL network (Au-  
202 tomatic monitoring network for littoral environment, Ifremer, France<sup>1</sup>).  
203 Such a system is based on the deployment of moored buoys equipped with  
204 physico-chemical measuring devices, working in continuous and autonomous  
205 conditions (Woerther, 1998; Blain et al., 2004). These stations use auto-  
206 matic systems for seawater analysis and real time data transmission. They  
207 record several parameters, such as temperature, salinity, dissolved oxygen,  
208 pH, and turbidity, with a fixed time resolution. The measuring station  
209 used here, the MAREL Carnot station, is situated in the eastern English  
210 Channel in the coastal waters of Boulogne-sur-mer (France) at position  
211 50.7404 N, 1.5676 W (Figure 1) and records data with a 20 minutes resolu-  
212 tion (Zongo et al., 2011). Water depth at this position varies between 5 and  
213 11 m; the measurements are done using a floating system inserted in a tube,  
214 1.5m below the surface. Statistical and scaling properties of MAREL auto-  
215 matic measurements in the English Channel have been studied previously,  
216 considering temperature time series (Dur et al., 2007) and turbidity, oxygen  
217 and pH (Schmitt et al., 2008) in the Seine estuary, and pH fluctuations in  
218 both the Seine estuary and Boulogne-sur-mer waters (Zongo and Schmitt,  
219 2011).

220 Among other parameters, the measuring buoy provides temperature,  
221 salinity and dissolved oxygen (DO) concentration data, as well as percentage

---

<sup>1</sup><http://www.ifremer.fr/marel>

222 of DO relative to the dissolved oxygen at equilibrium ( $SaO_2$ ) for the same  
 223 temperature and salinity. The DO time series is directly linked to temper-  
 224 ature due to the solubility equation given below, whereas  $SaO_2$  is free from  
 225 such direct influence. In the following, the latter dissolved oxygen series  
 226 is considered. The oxygen saturation percentage equation is given by Gar-  
 227 cia and Gordon, as a nonlinear function of the form (Garcia and Gordon,  
 228 1992):

$$SaO_2 = \frac{100DO}{\exp(P_1(T) + SP_2(T) + C_0S^2)} \quad (9)$$

229 where the denominator is the nonlinear fit expressing the oxygen solubility,  
 230  $S$  and  $T$  are salinity and temperature and  $P_1$  and  $P_2$  two polynomial de-  
 231 velopments ( $P_1$  of degree five, and  $P_2$  of degree three). Their coefficients  
 232 are given in Garcia and Gordon (1992).  $SaO_2$  data have thus no dimen-  
 233 sion and values exceeding 100 % correspond to supersaturation while values  
 234 below 100 % correspond to undersaturation associated to oxygen depletion;  
 235 values lower than 50 % are found for anoxic waters which can be dangerous  
 236 for many species.

237 Due to occasional failures in the measuring system, and to regular main-  
 238 tenance, the time series sampling frequency is not always 20 minutes; there  
 239 are frequently missing data and the mean sampling period is 24 minutes  
 240 for both data sets. A total of 145,587 data points for dissolved oxygen col-  
 241 lected from 25th May 2004 to 1st March 2011 and 155,825 data points for  
 242 sea temperature collected from 24th March 2004 to 1st March 2011 have  
 243 been analyzed. Figure 2 shows the two data sets. The temperature data  
 244 displays a strong annual cycle. These two data sets have been analyzed on  
 245 the same time period 25th May 2004 to 1st March 2011. There is a warm  
 246 winter in 2007 and 2008, showing also a weak oscillation of the temperature

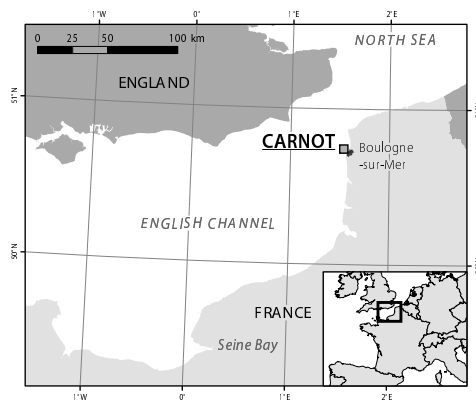


Figure 1: A map showing the measurement location Boullogne-sur-mer (France) at position 50.7404 N, 1.5676 W, in the eastern English Channel.

247 of the sea water.

248 The degree of stationary which was introduced by Chen et al. (2010) is

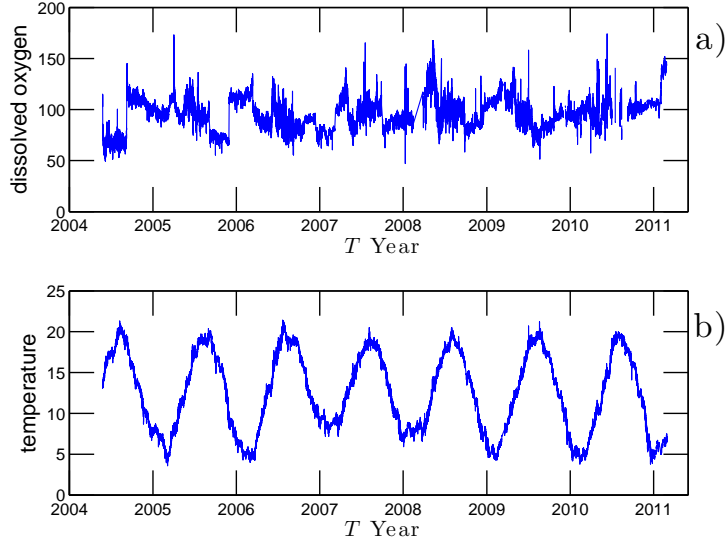


Figure 2: The observed dissolved oxygen a) and the temperature b) on the time period 25th May 2004 to 1st March 2011. Note that the sampling interval is not always 20 minutes, due to missing data. The mean period is 24 minutes for both data sets. A moderate warming winter is observed in 2007 and 2008. The observed temperature during the winter is 2 °C higher than usual. Note that a strong riding-wave phenomenon is observed from January to April 2008. The observed riding-wave will cause the mode mixing problem in the EMD decomposition.

249 first calculated, i.e.,

$$\mathcal{D}(\tau) = \text{std}(R(t_k^n, \tau)) \quad (10)$$

250 in which  $R(t_k^n, \tau)$  is an autocorrelation function with a sliding window  $t_k^n$  and  
 251 time delay  $\tau$ . The value of  $\mathcal{D}$  depends on the window size and the time delay  
 252  $\tau$ . It varies from 0 to 1 and characterizes the deviation from a stationary  
 253 process (Chen et al., 2010): 0 for exactly stationary processes and the larger  
 254 the value, the more it is non-stationary. Figure 3 shows the measured degree  
 255 of stationary  $\mathcal{D}$  for the autocorrelation and cross-correlation with a sliding  
 256 window size of  $t_w = 90$  days and  $t_w = 365$  days. To show the validation

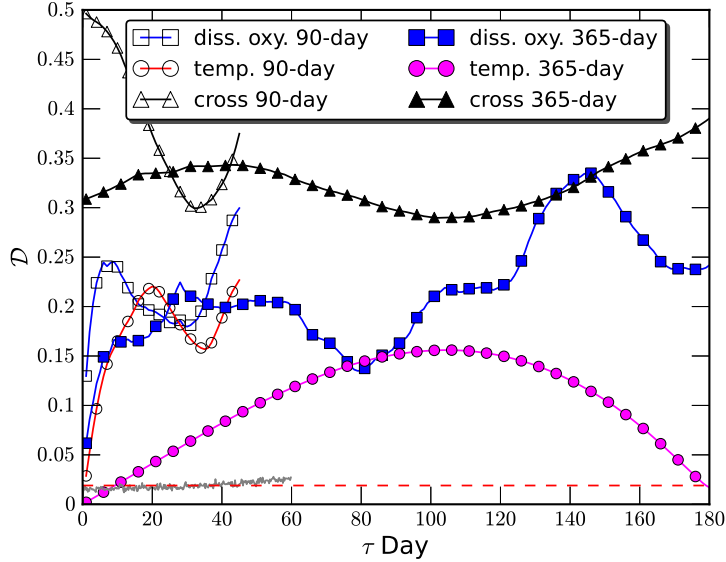


Figure 3: Statistical test of the degree of stationary  $\mathcal{D}$  for the autocorrelation and cross-correlation of two data sets with a sliding window  $t_w = 90$  days and  $t_w = 365$  days. The test for white noise is illustrated as a horizontal dashed line, showing the validation of the definition of the degree of stationary. Note that the measured  $\mathcal{D}$  is strongly dependent on the windows size  $t_w$ . The curves indicate that none of the series are stationary but that the temperate data set is more stationary than the dissolved oxygen one.

257 of Eq. (10), a test for white noise is performed, which is illustrated by a  
 258 dashed line. As expected a small value of  $\mathcal{D}$  is found for white noise. These  
 259 results applied on two experimental time series indicate that both are non-  
 260 stationary and that the temperature is more stationary than the dissolved  
 261 oxygen.

## 262 4. Analysis Results

### 263 4.1. Empirical Mode Decomposition Result

264 The EMD algorithm is applied to the two observed data sets for the  
 265 same time period without interpolating the data into a regular time inter-

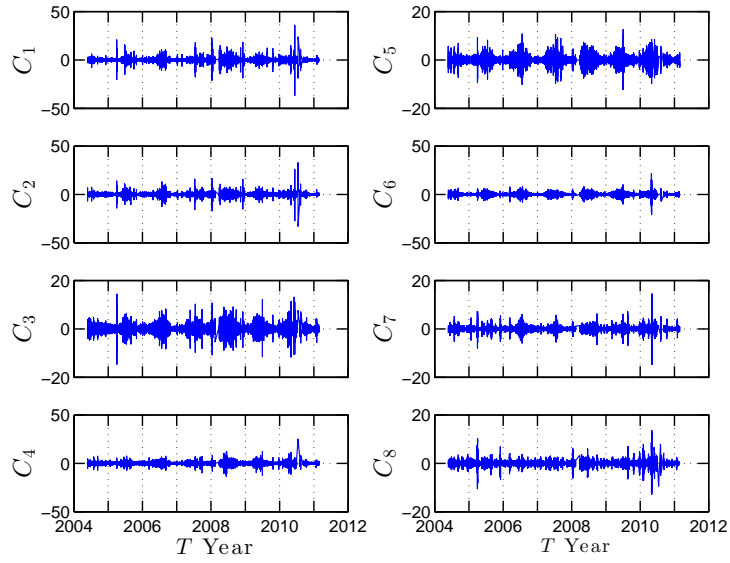


Figure 4: The first-eighth IMF modes for dissolved oxygen. The time scale is increasing with the mode index  $n$ .

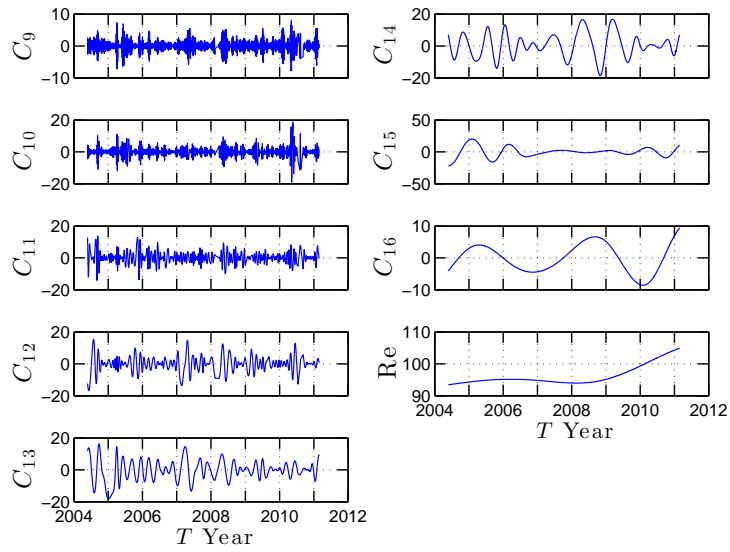


Figure 5: The last-eighth IMF modes for dissolved oxygen. The time scale is increasing with the mode index  $n$ .



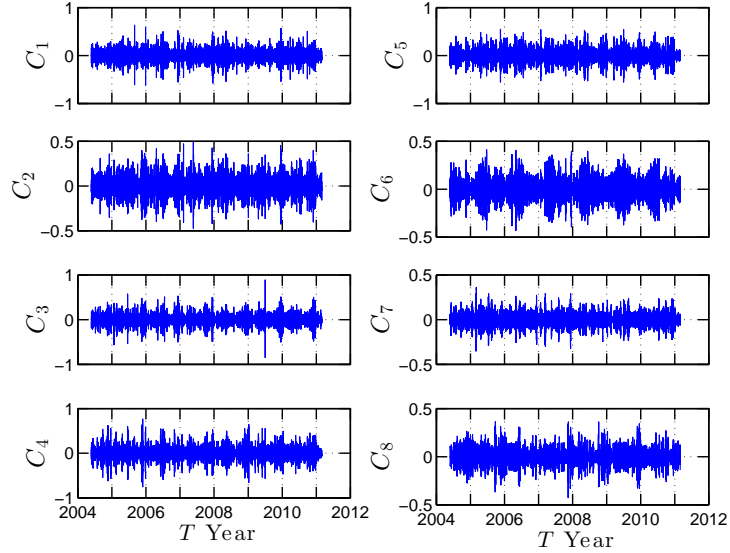


Figure 6: The first-eighth IMF modes for temperature. The time scale is increasing with the mode index  $n$ .

266 val, since in the EMD step the information is contained in the local extrema  
 267 points and can be applied to the time series with irregular time intervals  
 268 (Huang et al., 1998; Flandrin and Gonçalves, 2004). After the EMD de-  
 269 composition, there are respectively, 16 and 15 IMF modes with one residual  
 270 for the dissolved oxygen and temperature. Figures 4 to 7 show the corre-  
 271 sponding IMF modes. Note that the time scale is increasing with the index  
 272  $n$ : the number of the IMF mode. The IMF modes capture the local varia-  
 273 tion of the time scales. Note that there is a serious mode mixing problem  
 274 for the 13th IMF mode of the temperature around 2008, see Fig. 7. This  
 275 is caused by a riding-wave phenomenon in the original temperature data  
 276 (Huang et al., 1998), see Fig. 2 b. To eliminate the mode mixing problem, a  
 277 noise assistant method, namely Ensemble Empirical Mode Decomposition  
 278 (EEMD) could be applied to the data (Wu and Hunag, 2009). However,

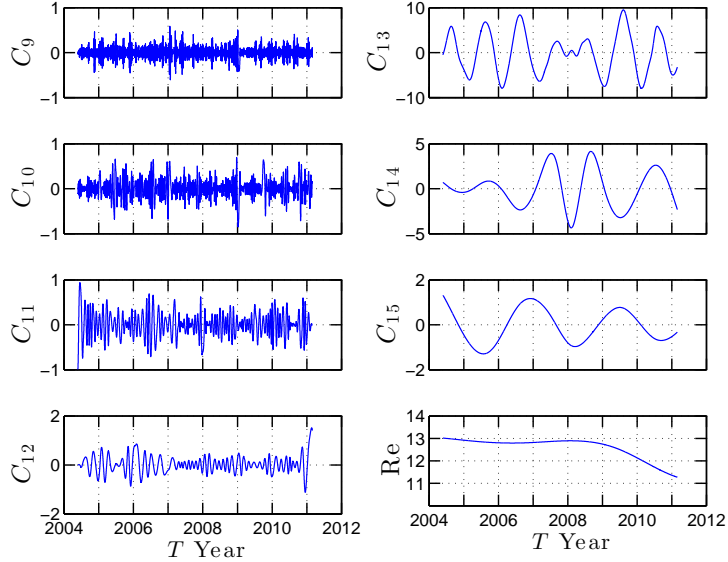


Figure 7: The last-seventh IMF modes together with the trend term for temperature. The time scale is increasing with the mode index  $n$ . Note that there is a serious mode mixing problem for the 13th IMF mode around 2008. The mean period of this mode is around 1 year. The mode mixing is caused by a riding-wave phenomenon from January 2008 to April with a typical time scale of 3 months, see Fig. 2 b.

279 practically speaking, the EEMD will introduce additional scales and bring  
 280 bias to the estimation of the Hilbert spectrum  $h(\omega)$ . Therefore the riding-  
 281 wave was removed manually. Figure 8 shows the last-seventh IMF modes  
 282 without the riding-wave: it provides a better 13th IMF mode. Note that  
 283 the trend term is not influenced by the riding-wave. The mean period of the  
 284 each IMF mode is estimated by calculating the local extrema points and  
 285 zero-crossing points (Rilling et al., 2003; Huang et al., 2009b), i.e.,

$$\bar{T}(n) = \frac{L}{N_{n,\max} + N_{n,\min} + N_{n,0}} \times 4 \quad (11)$$

286 in which  $L$  is the length of the data and  $n$  is the index. Figure 9 shows the  
 287 measured  $\bar{T}$  in a semilog plot. The first 12 IMF modes of the two data sets

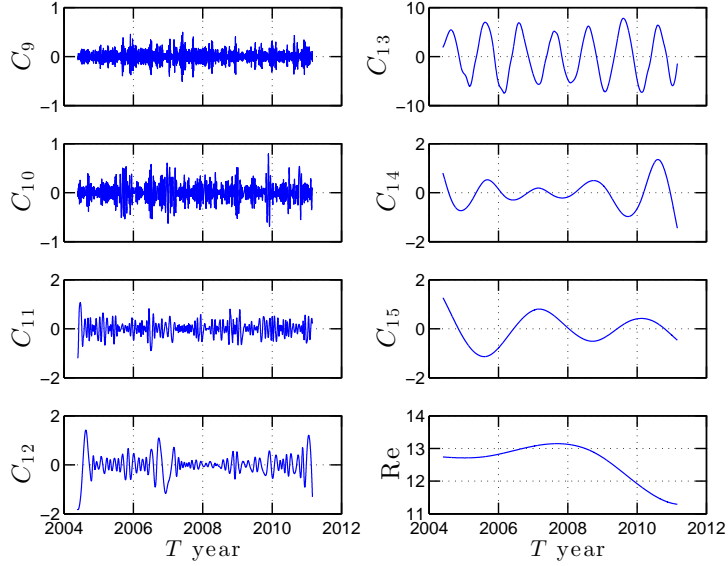


Figure 8: The last-seventh IMF modes together with the trend term for temperature by removing the riding-wave. A better annual cycle, i.e.,  $C_{13}$ , is obtained. Note that the trend is not influenced by removing the riding-wave.

288 approximately have the same mean period  $\bar{T}$  and follow an exponential law,  
 289 i.e.,

$$\bar{T}(n) = \alpha \times \gamma^n \quad (12)$$

290 in which  $\alpha \simeq 0.035$  and  $\gamma \simeq 1.78$  obtained by using a least square fitting  
 291 algorithm. This value is close to 2, which indicates a quasi dyadic filter  
 292 bank property of the EMD algorithm for these series, as found in other  
 293 situations (Wu and Huang, 2004; Flandrin et al., 2004; Huang et al., 2008,  
 294 2010). In other words, the mean scale of each mode series is 1.78 times the  
 295 mean scale of the previous one.

#### 296 4.2. Hilbert Spectrum

297 With the IMF modes obtained from EMD algorithm, the HSA can be  
 298 applied to each IMF mode. In this step, we first interpolate the IMF mode

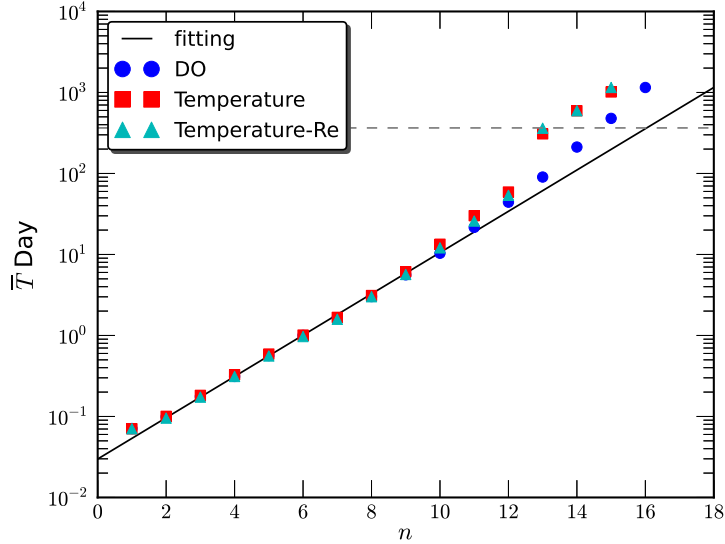


Figure 9: Mean period of IMF modes obtained for dissolved oxygen ( $\circ$ ), temperature with ( $\square$ ) and without ( $\triangle$ ) riding-wave, respectively. The annual cycle is indicated by a dashed line. A better annual cycle for the temperature is retrieved by removing the riding-wave. An exponential law is observed for both data sets with an exponent  $1.78 \pm 0.04$ , indicating a quasi dyadic-like filter bank of the EMD algorithm. Note that the first twelve IMF modes for both data sets approximately have the same mean period.

299 by using a Piecewise Cubic Hermite Interpolating Polynomial (phcip) algo-  
 300 rithm into a regular time interval with  $dt = 30$  minutes, which is slightly  
 301 larger than the mean time interval of 24 minutes. Then the HSA is applied  
 302 to extract the joint pdf  $p(\mathcal{A}, \omega)$ . The Hilbert marginal spectrum is then  
 303 calculated by using Eq. (7). Figure 10 shows the Hilbert marginal spec-  
 304 tra for dissolved oxygen ( $\circ$ ) and temperature ( $\square$ ), in which the vertical  
 305 line indicates the annual cycle. A strong annual cycle is observed for the  
 306 temperature data, which is consistent with the observation of the original  
 307 temperature data, see Fig. 2 b. It is emphasized here that for the tempera-  
 308 ture data with and without riding-wave around 2008, the Hilbert spectrum

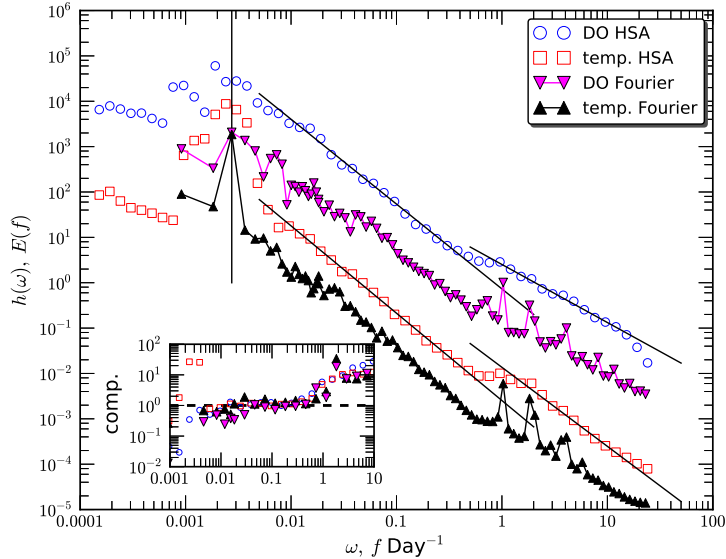


Figure 10: The Hilbert spectrum of dissolved oxygen ( $\circ$ ) and temperature ( $\square$ ), in which the vertical line indicates the annual cycle. Power law behavior is observed for both curves on the range  $0.01 < \omega < 0.5 \text{ day}^{-1}$  and  $2 < \omega < 20 \text{ day}^{-1}$ , corresponding to a time scale  $2 < T < 100 \text{ days}$  and  $1.2 < T < 12 \text{ hours}$ , respectively. The corresponding scaling exponents are  $1.93 \pm 0.05$  and  $1.87 \pm 0.08$  for large scales, and  $1.68 \pm 0.10$  and  $1.35 \pm 0.10$  for small scales respectively. For comparison, the Fourier power spectrum is also shown for both dissolved oxygen ( $\nabla$ ) and temperature ( $\triangle$ ). The inset shows the compensated spectrum  $h(\omega)\omega^2C^{-1}$  ( $E(f)f^2C^{-1}$ ) with fitted  $C$  to emphasize the observed power laws.

309  $h(\omega)$  are the same, showing the robustness of the present method. Power  
310 law behavior is observed on the frequency range  $0.01 < \omega < 0.5 \text{ day}^{-1}$ ,  
311 corresponding to time scales  $2 < T < 100 \text{ days}$  (resp.  $T = \omega^{-1}$ ), and  
312  $2 < \omega < 20 \text{ day}^{-1}$ , corresponding to time scales  $1.2 < T < 12 \text{ hours}$ . The  
313 measured scaling exponents are respectively  $1.93 \pm 0.05$  and  $1.87 \pm 0.08$  for  
314 the first scaling range of temperature and dissolved oxygen, and  $1.68 \pm 0.10$   
315 and  $1.35 \pm 0.10$  for the second scaling range. The scaling exponents for  
316 the first scaling range are statistically close to each other. For the second

317 scaling exponent, the temperature one is close to the Kolmogorov value  
 318  $5/3$  (Frisch, 1995), implying that the variation of the temperature within  
 319 one day is like a passive scalar. For comparison, the corresponding Fourier  
 320 power spectrum  $E(f)$  is also presented. Both Hilbert and Fourier spectra  
 321 show strong annual and daily cycles. However, there is no half-day cycle  
 322 observed in the Hilbert spectrum. It might indicate that the half-day cy-  
 323 cle is a harmonic from the nonlinear distortion of the daily cycle. Power  
 324 law behavior is also observed for the Fourier power spectrum on the same  
 325 range of time scales  $2 < T < 100$  days as for the Hilbert framework. The  
 326 corresponding scaling slope is close to 2. To emphasize the observed power  
 327 law behavior, the compensated spectra  $h(\omega)\omega^2C^{-1}$  (resp.  $E(f)f^2C^{-1}$ ) are  
 328 shown in the inset. The observed plateau confirms the power law. Note  
 329 that the observed  $-2$  power law indicates that there might be a cascade  
 330 process in the marine coastal environment (Thorpe, 2005). This should be  
 331 investigated further in future studies. Let us note that a shorter portion of  
 332 this data set has been studied in Zongo and Schmitt (2011): for the years  
 333 2006 to 2008, with about 50,000 data points, a Fourier analysis has found  
 334 a power-law slope of 1.66 for scales between 1 year and 2 hours, where the  
 335 fit was done for this whole range; it should be noted that different fits on  
 336 separated portions of the frequencies give values closer to the Hilbert-based  
 337 estimates.

### 338 *4.3. Time Dependent Intrinsic Correlation*

339 The correlation between these two data sets is considered here. Figure  
 340 11 displays the global cross correlation  $R(\tau)$  between the dissolved oxygen  
 341 and the temperature. There is a strong annual cycle with a 30 days phase

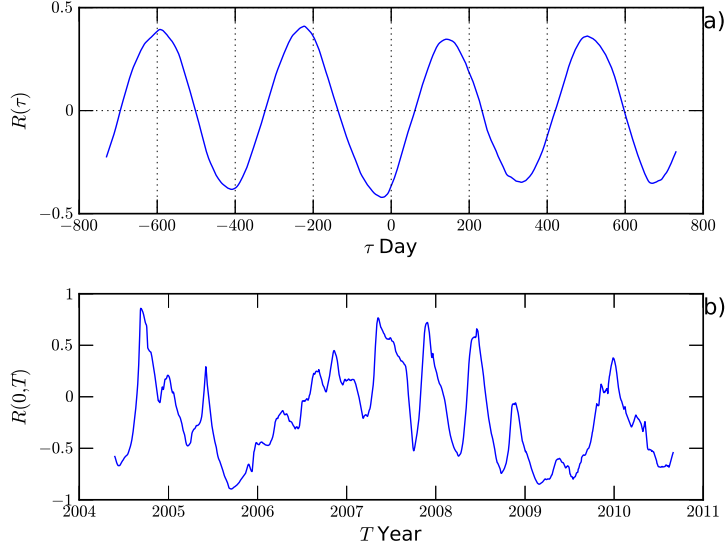


Figure 11: a) The global cross correlation coefficient  $R(\tau)$  between the dissolved oxygen and the temperature. Note that there is a strong annual cycle with a phase difference of 30 days. The global correlation coefficient is  $R(0) = -0.37 \pm 0.10$ . b) The measured cross correlation coefficient  $R(0, t_w)$  with a sliding window  $t_w = 180$  days. It shows that the relation between dissolved oxygen and temperature varies from time to time, indicating a multi-scale property of such data sets.

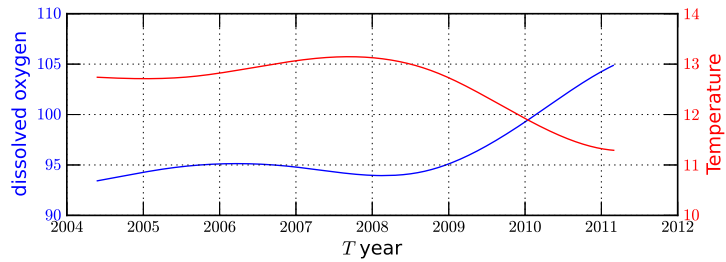


Figure 12: The trend from EMD for dissolved oxygen and temperature. The direct measurement of the cross correlation is  $-0.96$ , showing a global out-of-phase relation between the temperature and dissolved oxygen variation.

342 difference. The global correlation coefficient is found to be  $R(0) = -0.37 \pm$   
 343  $0.10$ . To show the variation of  $R$ , the cross correlation coefficient  $R(0, t_w)$

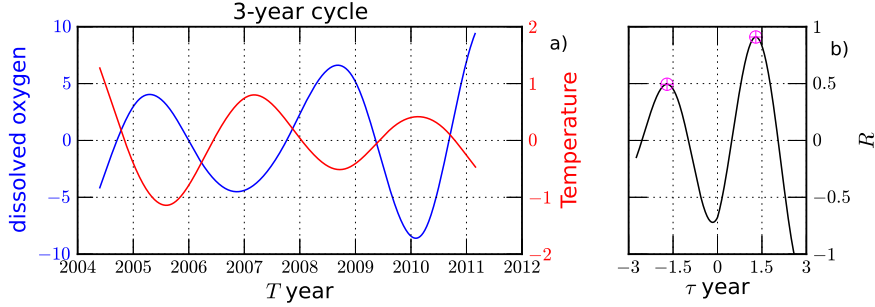


Figure 13: a) The IMF modes with a 3-year mean period. b) The measured cross correlation  $R(\tau)$ . They are negatively correlated with a phase difference of around 2 months. The overall correlation coefficient is  $R(0) = -0.68$ . The mean period is determined by the distance between the two local extrema points ( $\oplus$ ).

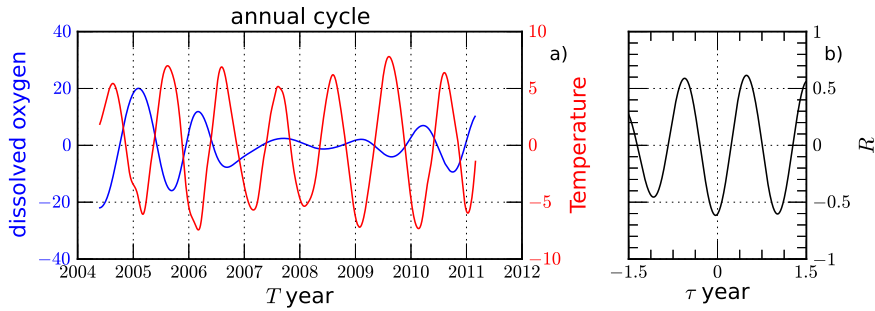


Figure 14: a) The annual cycle from EMD. b) The measured cross correlation  $R(\tau)$ . The overall correlation coefficient is  $R(0) = -0.60$  with 14 days phase difference. Note that there is a weak period between 2007 and 2009 for both temperature and dissolved oxygen.

344 is calculated with a sliding window  $t_w = 180$  days, which is shown in Fig.11  
 345 b. The standard deviation is found to be 0.40. Note that the standard  
 346 deviation as a measurement of the stationarity has been introduced, see  
 347 Eq. (10). It confirms that the global cross correlation coefficient ignores  
 348 the local/multi-scale information, which could be recovered by a proper  
 349 methodology (Chen et al., 2010).



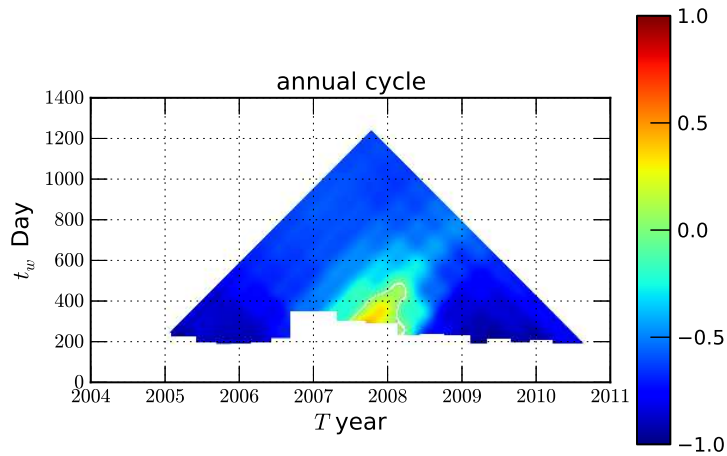


Figure 15: The measured TDIC for the annual cycle. It shows a transition from negative positive correlation between 2007 and 2008. The overall correlation coefficient is -0.60, see Fig. 14 b. The hole is the  $R$  cannot pass the  $t$ -test. The horizontal axis is the location of the centre of the sliding window.

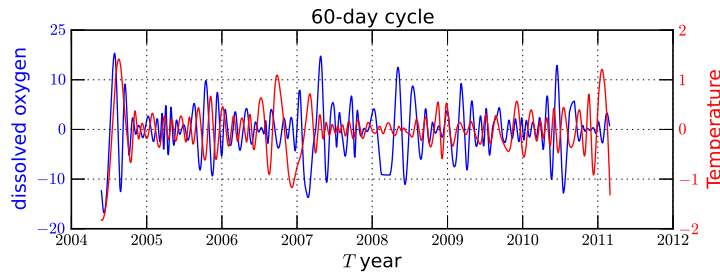


Figure 16: The 60-day cycle from EMD. The overall correlation coefficient is -0.02 with 15 days phase difference.

350 After the EMD decomposition, the data sets are represented in a multi-  
 351 scale way (Huang et al., 1998; Flandrin and Gonçalvès, 2004; Huang, 2009).  
 352 These are used for the multi-scale correlation analysis. Time scales larger  
 353 than or equal to one year are now considered. Figure 12 shows the residual  
 354 from the EMD algorithm, which has been recognized as the trend of the  
 355 given data (Wu et al., 2007; Moghtaderi et al., 2011). Figure 13 a) shows

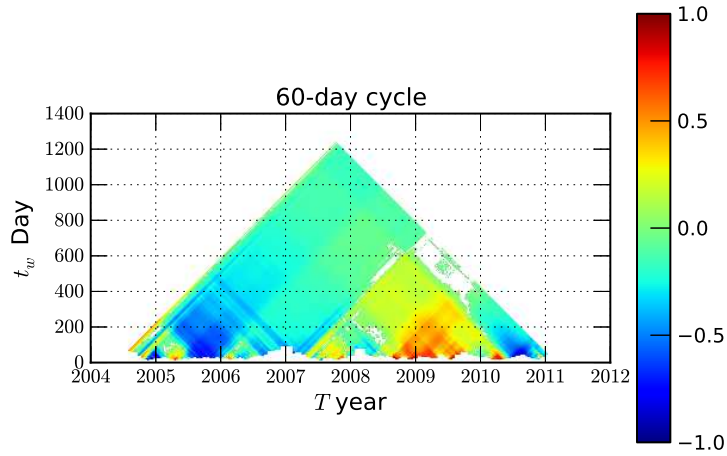


Figure 17: The measured TDIC for 60-day mean period. There is a more than half year strong correlation pattern around 2009 and 2010. The overall correlation coefficient is -0.02.

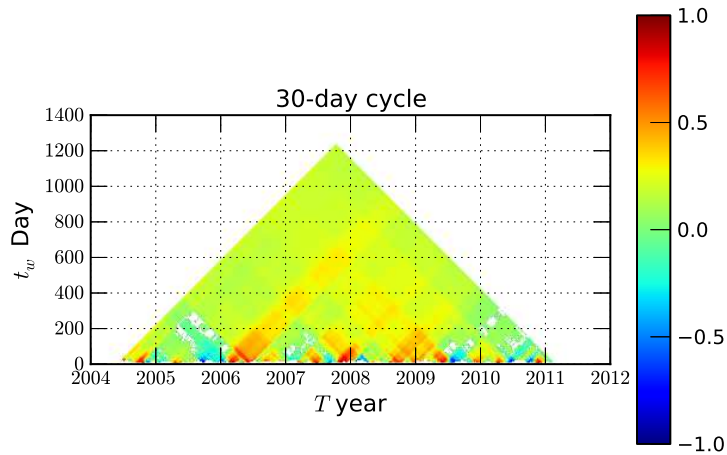


Figure 18: The measured TDIC for 30-day mean period on the range May 2004 ~ January 2008. There are more than half a years strong correlation patterns between January 2006 and June 2006. The overall correlation coefficient is 0.17.

356 the IMF modes with a 3-year mean period, and Figure 13 b) the correspond-  
 357 ing cross correlation  $R(\tau)$ . They show a negative correlation with each other  
 358 with a phase difference of 2 months. Figure 14 a) shows the annual cycle

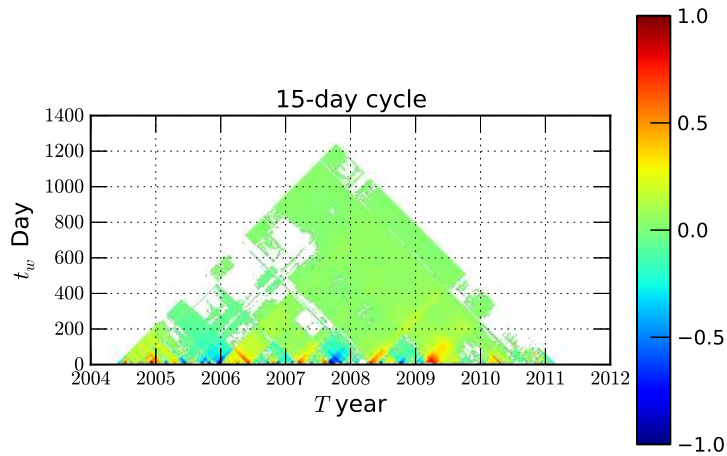


Figure 19: The measured TDIC for the 15-day mean period. The overall correlation coefficient is 0.10.

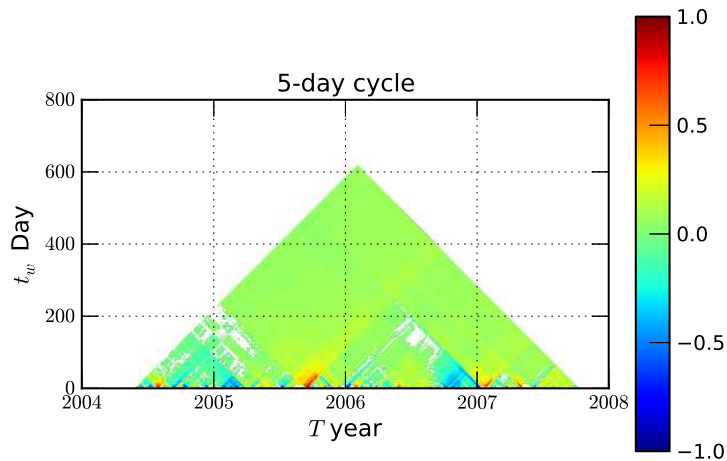


Figure 20: The measured TDIC for the 5-day mean period. The overall correlation coefficient is 0.1.

359 from EMD, Figure 14 b) the corresponding cross correlation  $R(\tau)$ . Again  
 360 they are negatively correlated with each other. The overall correlation co-  
 361 efficient is -0.63 with a 14 day phase difference. An interesting observation  
 362 is that there is a weak period between 2007 and 2009 for both data sets,  
 363 indicating that a special event has happened. The measured TDIC is shown

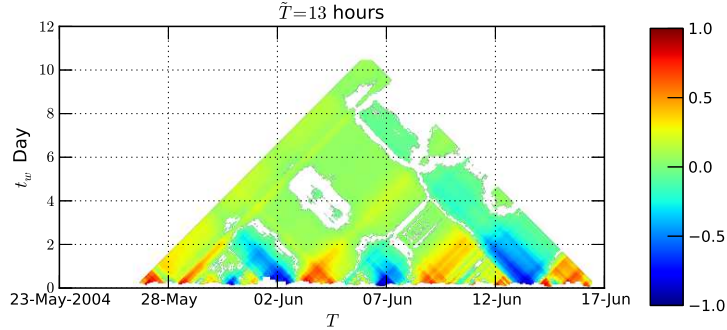


Figure 21: The measured TDIC for the 13-day mean period. The overall correlation coefficient is 0.1. The holes indicate that the measured TDIC can not pass the  $t$ -test.

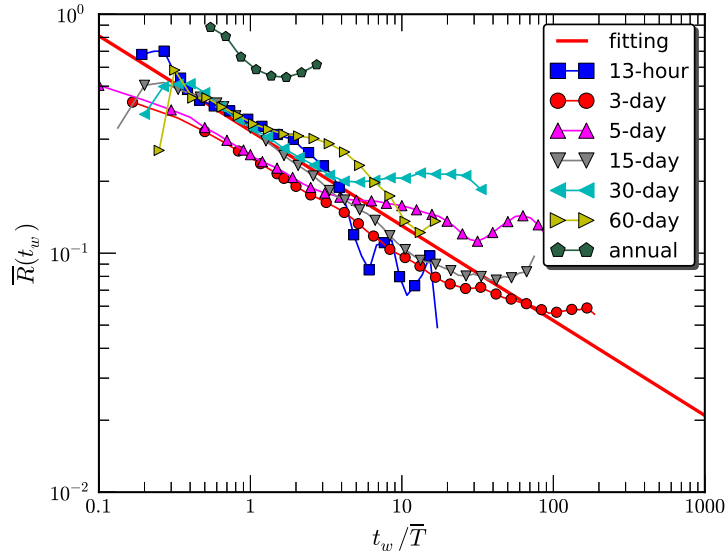


Figure 22: The measured absolute mean value  $\bar{R}(t_w)$  for different time scales  $\bar{T}$ . For display clarity, the sliding window  $t_w$  is normalized by their own mean period  $\bar{T}$ . Power law behavior is observed on the  $0.4 < t_w/\bar{T} < 4$  with a scaling exponent  $0.40 \pm 0.01$ .

364 in Figure 15. There is a positive correlation around 2008. The transition  
 365 from negative (resp. out-of-phase) to positive (in-phase) and again to neg-  
 366 ative correlation from mid of 2007 to the mid of 2008 might be an effect of  
 367 the warming from mid 2007 until almost 2009. During this period, the sea

368 water temperature was consequently 2°C higher than usual in the winter  
 369 time. Therefore, the out-of-phase relation between DO and temperature is  
 370 affected by this event.

371 Let us consider scales less than one year. Figure 16 shows the IMF  
 372 modes with a mean period of 60 days. They are positively correlated with  
 373 each other on some portions and negatively correlated on others, showing  
 374 rich dynamics. However, the overall correlation coefficient is small (resp.  
 375  $-0.02$ ). Figure 17 displays the measured TDIC, which confirms the direct  
 376 observation of the IMF modes. A strong positive correlation is observed  
 377 during the time period 2009~2010. Due to the complexity of the coastal  
 378 environment system, the exact reason for this changes from negative to  
 379 positive is unclear. It will be addressed in future studies. For time scales  
 380 smaller than 60 days, the original IMF are not shown here, but only the  
 381 measured TDIC. Figure 18~21 show the measured TDIC for mean periods  
 382 of 30-day to 13-hour respectively. All TDICs show rich patterns at a small  
 383 sliding window. Let us also note that with the increase of the window size  
 384 they decorrelate. To show the decorrelation of the TDIC, a absolute mean  
 385 value of the measured  $R_i(t_k^n)$  is defined, i.e.,

$$\overline{R}(t_w) = \langle |R(t_k^n, t_w)| \rangle_t \quad (13)$$

386 Figure 22 shows in a log-log plot of the measured  $\overline{R}(t_w)$  for seven time scales  
 387 considered above. Note that the horizontal axis  $t_w$  has been normalized by  
 388 their mean period  $\overline{T}$ . Generally speaking, the curves are decreasing with  
 389 the increasing of the sliding window size  $t_w/\overline{T}$ , showing the decorrelation  
 390 between dissolved oxygen and temperature on different scales. A power law

391 behavior is observed on  $0.4 < t_w/\bar{T} < 4$ , i.e.,

$$\bar{R} \sim (t_w/\bar{T})^{-\alpha} \quad (14)$$

392 with a scaling exponent  $\alpha = 0.40 \pm 0.10$  obtained by using a least square  
393 fitting algorithm. This indicates that the considered modes decorrelate with  
394 each other in a power law way, with the same law.

## 395 5. Conclusion

396 Marine environmental time series can be quite complex, especially with  
397 the influence of turbulent stochastic fluctuations, multi-scale dynamics, and  
398 deterministic forcings. Such time series are as a result often non stationary  
399 and nonlinear. It has been shown elsewhere that the EMD method, together  
400 with Hilbert spectral analysis, is less influenced by deterministic forcing  
401 than other methods (Huang et al., 2010, 2011). Here this approach was  
402 applied to automatic temperature and oxygen data. Power law spectra was  
403 found using Hilbert spectral analysis. Both series have similar spectra over  
404 the range from 2 to 100 days, whereas there is a difference in slopes for high  
405 frequency power law regimes. The time evolution and scale dependence of  
406 cross correlations between both series were considered. The decomposition  
407 into modes helped to estimate how correlations vary among scales. It was  
408 found that the trends are perfectly anti-correlated, and that the modes of  
409 mean year 3 years and 1 year have also negative correlation, whereas higher  
410 frequency modes have a much smaller correlation. A new methodology was  
411 also applied, time-dependent intrinsic correlations: this showed the patterns  
412 of correlations at different scales, for different modes.

413 Such analysis may help to identify some key mechanisms. Here a strong  
414 anti-correlation was found for modes of mean time scale of 3 years, with a  
415 phase shift of 2 months. An explanation of such a result could be that, at  
416 these scales, higher temperatures may favour larger phytoplankton growth  
417 rate, and hence, with a time delay, a lower percentage of oxygen. Of course  
418 such relations are not always true, and the color maps of TDIC reveal the  
419 variations of the strength of such relationship.

420 While Fourier space methods can produce in some respects similar re-  
421 sults for the power spectra, cross-correlations through co-spectra, and some  
422 colour maps of correlations in frequency space, they do not provide time-  
423 frequency information like the EMD based method used here. Furthermore,  
424 the TDIC tested here is a new method for correlation analysis that could be  
425 applied on other time series from the environmental and oceanic sciences,  
426 since in these fields time series are typically complex, with fluctuations at  
427 all scales, and nonlinear and non stationary features.

## 428 **Acknowledgements**

429 This work is sponsored in part by the National Natural Science Foun-  
430 dation of China (Nos. 11072139, 11032007 and 11202122), and ‘Pu Jiang’  
431 project of Shanghai (No. 12PJ1403500) and the Shanghai Program for In-  
432 novative Research Team in Universities. The EMD MATLAB codes used in  
433 this study are written by Dr Gabriel Rilling and Prof. Patrick Flandrin from  
434 the laboratoire de Physique, CNRS & ENS Lyon (France): <http://perso.ens-lyon.fr/patrick.flandrin/emd.html>. We thank Ifremer, and especially Alain  
435 Lefebvre and Michel Repecaud for their work in recording and validating  
436 the Marel data. We thank the I. Puillat and the others organizers of the  
437

438 Time Series Brest conference for a very nice meeting, and the reviewers  
439 for useful comments and suggestions. We thank also Denis Marin (LOG,  
440 Dunkerque, France) for the realization of Figure 1.

## 441 **References**

## 442 **References**

- 443 Best, M., Wither, A., Coates, S., 2007. Dissolved oxygen as a physico-chemical supporting  
444 element in the water framework directive. *Marine Pollution Bulletin* 55, 53–64.
- 445 Blain, S., Guillou, J., Treguer, P., Woerther, P., Delauney, L., Follenfant, E., Gontier, O.,  
446 Hamon, M., Leilde, B., Masson, A., Tartub, C., Vuillemin, R., 2004. High frequency  
447 monitoring of the coastal environment using the marel buoy. *J. Environ. Monitoring*  
448 6, 569–575.
- 449 Chang, G., Dickey, T., 2001. Optical and physical variability on timescales from minutes  
450 to the seasonal cycle on the new england shelf: July 1996 to june 1997. *J. Geophys.*  
451 *Res.* 106, 9435–9453.
- 452 Chavez, et al., 1997. Moorings and drifters for real-time interdisciplinary oceanography.  
453 *J. Atmos. Ocean. Technol.* 14, 1199–1211.
- 454 Chen, X., Wu, Z., Huang, N. E., 2010. The time-dependent intrinsic correlation based  
455 on the empirical mode decomposition. *Adv. Adapt. Data Anal* 2, 233–265.
- 456 Cohen, L., 1995. *Time-frequency analysis*. Prentice Hall PTR Englewood Cliffs, NJ.
- 457 Coughlin, K. T., Tung, K. K., 2004. 11-Year solar cycle in the stratosphere extracted by  
458 the empirical mode decomposition method. *Adv. Space Res.* 34 (2), 323–329.
- 459 Dätig, M., Schlurmann, T., 2004. Performance and limitations of the hilbert–huang trans-  
460 formation (hht) with an application to irregular water waves. *Ocean Eng.* 31 (14),  
461 1783–1834.
- 462 Dickey, T., 1991. The emergence of concurrent high resolution physical and bio-optical  
463 measurements in the upper ocean and their applications. *Rev. Geophys.* 29, 383–413.
- 464 Dur, G., Schmitt, F. G., Souissi, S., 2007. Analysis of high frequency temperature time  
465 series in the seine estuary from the marel autonomous monitoring buoy. *Hydrobiologia*  
466 588.



- 467 Echeverria, J. C., Crowe, J. A., Woolfson, M. S., Hayes-Gill, B. R., 2001. Application  
468 of empirical mode decomposition to heart rate variability analysis. *Med. Biol. Eng.*  
469 *Comput.* 39 (4), 471–479.
- 470 Flandrin, P., 1998. *Time-frequency/time-scale analysis*. Academic Press.
- 471 Flandrin, P., Gonçalves, P., 2004. Empirical Mode Decompositions as Data-Driven  
472 Wavelet-Like Expansions. *Int. J. Wavelets, Multires. Info. Proc.* 2 (4), 477–496.
- 473 Flandrin, P., Rilling, G., Gonçalves, P., 2004. Empirical mode decomposition as a filter  
474 bank. *IEEE Sig. Proc. Lett.* 11 (2), 112–114.
- 475 Frisch, U., 1995. *Turbulence: the legacy of AN Kolmogorov*. Cambridge University Press.
- 476 Garcia, H. E., Gordon, L. I., 1992. Oxygen solubility in seawater: better fitting equations.  
477 *Limnology and Oceanography* 37, 1307–1312.
- 478 Hoover, K., 2003. non-stationary time series cointegration and the principle of the  
479 common cause. *British J. Philosophy Sci.* 54, 527–551.
- 480 Huang, N. E., 2005. *Hilbert-Huang Transform and Its Applications*. World Scientific, Ch.  
481 1. Introduction to the Hilbert-Huang transform and its related mathematical problems,  
482 pp. 1–26.
- 483 Huang, N. E., Shen, Z., Long, S. R., 1999. A new view of nonlinear water waves: The  
484 Hilbert Spectrum . *Annu. Rev. Fluid Mech.* 31 (1), 417–457.
- 485 Huang, N. E., Shen, Z., Long, S. R., Wu, M. C., Shih, H. H., Zheng, Q., Yen, N., Tung,  
486 C. C., Liu, H. H., 1998. The empirical mode decomposition and the Hilbert spectrum  
487 for nonlinear and non-stationary time series analysis. *Proc. R. Soc. London, Ser. A*  
488 454 (1971), 903–995.
- 489 Huang, N. E., Wu, Z., Long, S., Arnold, K., Chen, X., Blank, K., 2009a. On instantaneous  
490 frequency. *Adv. Adapt. Data Anal* 1 (2), 177–229.
- 491 Huang, Y., 2009. *Arbitrary-order hilbert spectral analysis: Definition and application to*  
492 *fully developed turbulence and environmental time series*. Ph.D. thesis, Université des  
493 *Sciences et Technologies de Lille - Lille 1, France & Shanghai University, China.*
- 494 Huang, Y., Schmitt, F., Lu, Z., Fougairolles, P., Gagne, Y., Liu, Y., 2010. Second-order  
495 structure function in fully developed turbulence. *Phys. Rev. E* 82 (2), 026319.
- 496 Huang, Y., Schmitt, F., Lu, Z., Liu, Y., 2008. An amplitude-frequency study of turbulent  
497 scaling intermittency using hilbert spectral analysis. *Europhys. Lett.* 84, 40010.

- 498 Huang, Y., Schmitt, F., Lu, Z., Liu, Y., 2009b. Analysis of daily river flow fluctuations  
499 using empirical mode decomposition and arbitrary order hilbert spectral analysis. *J.*  
500 *Hydrol.* 373, 103–111.
- 501 Huang, Y., Schmitt, F. G., Hermand, J.-P., Gagne, Y., Lu, Z., Liu, Y., 2011. Arbitrary-  
502 order Hilbert spectral analysis for time series possessing scaling statistics: comparison  
503 study with detrended fluctuation analysis and wavelet leaders. *Phys. Rev. E* 84 (1),  
504 016208.
- 505 Hwang, P. A., Huang, N. E., Wang, D. W., 2003. A note on analyzing nonlinear and  
506 non-stationary ocean wave data. *Appl. Ocean Res.* 25 (4), 187–193.
- 507 János, I., Müller, R., 2005. Empirical mode decomposition and correlation properties of  
508 long daily ozone records. *Phys. Rev. E* 71 (5), 56126.
- 509 Long, S. R., Huang, N. E., Tung, C. C., Wu, M. L., Lin, R. Q., Mollo-Christensen, E.,  
510 Yuan, Y., 1995. The Hilbert techniques: an alternate approach for non-steady time  
511 series analysis. *IEEE Geoscience and Remote Sensing Soc. Lett.* 3, 6–11.
- 512 Loutridis, S. J., 2004. Damage detection in gear systems using empirical mode decom-  
513 position. *Eng. Struct.* 26 (12), 1833–1841.
- 514 Moghtaderi, A., Borgnat, P., Flandrin, P., 2011. Trend filtering: empirical mode decom-  
515 positions versus  $\ell_1$  and hodrick–prescott. *Adv. Adapt. Data Anal* 3 (01n02), 41–61.
- 516 Molla, M. K. I., Rahman, M. S., Sumi, A., Banik, P., 2006a. Empirical mode decomposi-  
517 tion analysis of climate changes with special reference to rainfall data. *Discrete Dyn.*  
518 *Nat. Soc.* 2006, Article ID 45348, 17 pages, doi:10.1155/DDNS/2006/45348.
- 519 Molla, M. K. I., Sumi, A., Rahman, M. S., 2006b. Analysis of Temperature Change  
520 under Global Warming impact using Empirical Mode Decomposition . *Int. J. Info.*  
521 *Tech.* 3 (2), 131–139.
- 522 Papadimitriou, S., Sun, J., Yu, P. S., 2006. Local correlation tracking in time series.  
523 *Proc. Sixth Int. Conf. Data Mining*, 456-465.
- 524 Rilling, G., Flandrin, P., Gonçalvès, P., 2003. On empirical mode decomposition and its  
525 algorithms. *IEEE-EURASIP Workshop on Nonlinear Signal and Image Processing*.
- 526 Rodo, X., Rodriguez-Arias, M. A., 2006. A new method to detect transitory signatures  
527 and local time/space variability structures in the climate system: the scale-dependent  
528 correlation analysis. *Clim. Dyn.* 27, 441–458.

- 529 Schmitt, F. G., Huang, Y., Lu, Z., Liu, Y., Fernandez, N., 2009. Analysis of velocity  
530 fluctuations and their intermittency properties in the surf zone using empirical mode  
531 decomposition. *J. Mar. Sys.* 77, 473–481.
- 532 Schmitt, F. G., Dur, G., Souissi, S., Brizard Zongo, S., 2008. Statistical properties of  
533 turbidity, oxygen and pH fluctuations in the Seine river estuary (France). *Physica A*  
534 387 (26), 6613–6623.
- 535 Thorpe, S. A., 2005. *The turbulent ocean*. Cambridge University Press.
- 536 Veltcheva, A. D., Soares, C. G., 2004. Identification of the components of wave spectra  
537 by the Hilbert Huang transform method. *Appl. Ocean Res.* 26 (1-2), 1–12.
- 538 Woerther, P., 1998. Marel: Mesures automatisées en réseau pour l’environnement littoral.  
539 Léau, Les industrie, Les nuisances 217, 67–72.
- 540 Wu, Z., Huang, N. E., 2004. A study of the characteristics of white noise using the  
541 empirical mode decomposition method. *Proc. R. Soc. London, Ser. A* 460, 1597–1611.
- 542 Wu, Z., Huang, N. E., Long, S. R., Peng, C., 2007. On the trend, detrending, and  
543 variability of nonlinear and non-stationary time series. *PNAS* 104 (38), 14889.
- 544 Wu, Z., Hunag, N. E., 2009. Ensemble empirical mode decomposition: a noise-assisted  
545 data analysis method. *Adv. Adapt. Data Anal.* 1, 1–41.
- 546 Zhu, X., Shen, Z., Eckermann, S. D., Bittner, M., Hirota, I., Yee, J. H., 1997. Grav-  
547 ity wave characteristics in the middle atmosphere derived from the empirical mode  
548 decomposition method. *J. Geophys. Res* 102, 16545–16561.
- 549 Zongo, S., Schmitt, F., Lefebvre, A., 2011. Observations biogéochimiques des eaux  
550 côtières à boulogne-sur-mer à haute fréquence: les mesures automatiques de la bouée  
551 marel., in *Du naturalisme à l’écologie*, édité par F.G. Schmitt, Presses de l’UOF, 253–  
552 266.
- 553 Zongo, S. B., Schmitt, F. G., 2011. Scaling properties of pH fluctuations in coastal  
554 waters of the english channel: pH as a turbulent active scalars. *Nonlinear Processes*  
555 *in Geophysics* 18, 829–839.

